Redox Biology 22 (2019) 101129

Contents lists available at ScienceDirect

Redox Biology

journal homepage: www.elsevier.com/locate/redox

Research Paper

Lung epithelial protein disulfide isomerase A3 (PDIA3) plays an important role in influenza infection, inflammation, and airway mechanics

Nicolas Chamberlain[a], Bethany R. Korwin-Mihavics[a], Emily M. Nakada[a], Sierra R. Bruno[a], David E. Heppner[a], David G. Chapman[b,d,e,f], Sidra M. Hoffman[a], Albert van der Vliet[a], Benjamin T. Suratt[b], Oliver Dienz[c], John F. Alcorn[g], Vikas Anathy[a,*]

[a] Department of Pathology and Laboratory Medicine, University of Vermont College of Medicine, Burlington, VT, United States
[b] Department of Medicine, University of Vermont College of Medicine, Burlington, VT, United States
[c] Department of Surgery, University of Vermont College of Medicine, Burlington, VT, United States
[d] Woolcock Institute of Medical Research, University of Sydney, Sydney, Australia
[e] Sydney Medical School, University of Sydney, Sydney, Australia
[f] Translational Airways Group, School of Life Sciences, University of Technology, Sydney, Australia
[g] Division of Pulmonary Medicine, Allergy, and Immunology, Department of Pediatrics, Children's Hospital of Pittsburgh of UPMC, University of Pittsburgh, Pittsburgh, PA, United States

A B S T R A C T

Protein disulfide isomerases (PDI) are a family of redox chaperones that catalyze formation or isomerization of disulfide bonds in proteins. Previous studies have shown that one member, PDIA3, interacts with influenza A virus (IAV) hemagglutinin (HA), and this interaction is required for efficient oxidative folding of HA *in vitro*. However, it is unknown whether these host-viral protein interactions occur during active infection and whether such interactions represent a putative target for the treatment of influenza infection. Here we show that PDIA3 is specifically upregulated in IAV-infected mouse or human lung epithelial cells and PDIA3 directly interacts with IAV-HA. Treatment with a PDI inhibitor, LOC14 inhibited PDIA3 activity in lung epithelial cells, decreased intramolecular disulfide bonds and subsequent oligomerization (maturation) of HA in both H1N1 (A/PR8/34) and H3N2 (X31, A/Aichi/68) infected lung epithelial cells. These reduced disulfide bond formation significantly decreased viral burden, and also pro-inflammatory responses from lung epithelial cells. Lung epithelial-specific deletion of PDIA3 in mice resulted in a significant decrease in viral burden and lung inflammatory-immune markers upon IAV infection, as well as significantly improved airway mechanics. Taken together, these results indicate that PDIA3 is required for effective influenza pathogenesis *in vivo*, and pharmacological inhibition of PDIs represents a promising new anti-influenza therapeutic strategy during pandemic and severe influenza seasons.

1. Introduction

Viruses harness their host cell transcriptional machinery and endoplasmic reticulum (ER) to express and properly fold and mature virus proteins, respectively [1]. Viral proteins often rely on the redox-dependent formation of disulfide bonds (-S-S-) for stability and function [2]. In general disulfide bonds within membrane and secretory proteins are constructed in the ER and require ER-localized oxidoreductases [3–5]. One of these oxidoreductases is protein disulfide isomerase (PDI) A3, which belongs to a family of PDIs that catalyze formation and isomerization of disulfide bonds within nascent peptides in the ER [6,7]. PDIA3 is unique among other PDIs in that it has an enhanced specificity towards glycoproteins owing to its interactions with calreticulin and calnexin, two lectin binding chaperone proteins within the ER [8]. In addition to numerous roles with in the cell, recent studies have linked PDIA3 with various cancers and the onset of neurodegenerative disorders [9,10], though its role during viral infection is less well studied.

Influenza specifically infects and replicates in lung epithelial cells due to the presence of compatible sialic acid residues that can bind to influenza hemagglutinin (HA) [11,12]. Previous work has shown that influenza HA contains several disulfide bonds and traverses through the ER to attain its final conformation via ER based folding and glycosylation [13,14]. PDIA3 has been shown to interact with IAV-HA and to facilitate disulfide bond formation in HA during its passage through the ER [15]. It is also evident that these disulfide bonds formed by PDIA3 are essential for HA activity *in vitro* [15–17]. Despite *in vitro* evidence it is not well established whether PDIA3 is required for viral burden *in vivo*, nor is it known about the effect of PDIA3 deletion has on the disulfide status and maturation of HA during active IAV infection in primary lung epithelial cells and in mouse lungs.

In this study, we observed that PDIA3 is specifically upregulated in

* Corresponding author.
E-mail address: vikas.anathy@med.uvm.edu (V. Anathy).

https://doi.org/10.1016/j.redox.2019.101129
Received 14 December 2018; Received in revised form 24 January 2019; Accepted 28 January 2019
Available online 29 January 2019

IAV-infected lung epithelial cells and mouse lungs as compared to other PDI family members. Additionally, the newly discovered small molecule inhibitor of PDI, [18] LOC14 exhibited the capacity to inhibit recombinant (r)PDIA3 at an IC50 of approximately 5 μM. Treatment of IAV-infected primary mouse tracheal epithelial cells (MTECs) with LOC14 resulted in decreased viral burden and pro-inflammatory cytokine production. IAV-HA showed a deficiency in disulfide bonds in cells treated with LOC14. Furthermore, this deficiency of disulfide bonds also decreased mature IAV-HA, indicating that PDI inhibition affects HA maturation within the host cell. Following influenza infection, mice with lung epithelium-specific knockout of *Pdia3* showed decreased overall viral burden, reduced inflammation and improved lung mechanics.

2. Results

2.1. PDIA3 expression is increased following IAV infection

Wild type (C57BL/6NJ-*WT*) mice were infected with 2000 egg infectious units (EIU) of influenza A virus (IAV) strain H1N1 (PR8) and lung lysates were analyzed for PDI expression. Six days post infection a significant increase in *Pdia3* transcripts were observed when compared to other *Pdia* gene transcripts (Fig. 1A). Mice infected with replication-deficient, UV irradiated (mock) virus, did not show any increases in *Pdia3*, suggesting the *Pdia3* induction depends on active viral replication. We next examined PDIA3 protein expression in the lung sections of PR8 infected *WT* mice, and observed a marked increase in PDIA3 levels predominantly in the bronchial epithelial cells in mice infected with PR8 compared to mock treated mice (Fig. 1B). Next, we sought to determine if this increase following IAV infection was exclusive to PR8 H1N1 or also prevalent in other influenza strains. Shoemaker et al. [19] have performed microarray using lung homogenates of mice infected with various strains of influenza virus, to examine gene expression over different time points. A retrospective analysis of this microarray data set (GSE63786) revealed *Pdia3* is the only *Pdi* significantly upregulated compared to uninfected controls at 72 h, 120 h, and 168 h post infection with various strains of IAV (Fig. 1C & S1). A similar microarray experiment was performed by Gerlach et al. [20] in human lung epithelial cells 36 h post infection and a retrospective analysis of this data set (GSE48466) also revealed significantly upregulated *PDIA3* in response to pandemic influenza infection (Fig. 1D). Despite increased expression of *PDIA3* in response to seasonal influenza infection, this was not found to be statistically significant (Fig. 1D).

PDIA3 is known to interact with the hemagglutinin (HA) protein of IAV to construct disulfide bonds (-S-S-) in HA of IAV [15]. We performed immunoprecipitations (IPs) in human bronchial epithelial (HBE) cells after IAV infection. Upon analysis of the immunoprecipitated samples by western blot, we found both increased PDIA3 expression, as well as high levels of HA co-immunoprecipitating with PDIA3 (Fig. 1E). Western blots of whole cell lysate (WCL) showed trends in increases in HA and PDIA3, and no alterations in GAPDH were observed (Fig. 1E and Fig S1,B). Next, we knocked down PDIA3 using siRNA and then lung epithelial cells were infected with IAV or mock virus. Subsequent Western blot analysis showed that knockdown of PDIA3 decreased levels of HA in IAV infected cells as compared to scrambled siRNA transfected cells (Fig. 1F and Fig S1C). These results suggest following IAV infection PDIA3 is predominantly induced in human and mouse lung epithelial cells, and siRNA mediated decrease in PDIA3 expression diminish IAV-HA production in lung epithelial cells.

2.2. PDI inhibitors decrease PDIA3 activity and influenza protein production

PDIs play important roles in the folding of cellular proteins, and the prototypical PDI, PDIA1, has been found to be implicated in numerous diseases [21]. As such there are several commercially available small molecule inhibitors that target PDIA1, while little is known regarding the effect of these inhibitors on other PDIs. It is presumed that these inhibitors will have inhibitory effect on other PDIs owing to the high conservation of a thioredoxin-like (CXXC) active site and the high degree of homology between protein binding domains of the various PDI family members [18,22–24]. We therefore tested four PDI inhibitors: 16F16, LOC14, PACMA31, and CCF 642, all extensively characterized as inhibitors of PDIA1, for their efficacy to inhibit PDIA3. Reduction of Dieosine-diglutathione (DiE-GSSG) has been used as an assay to determine PDI activity [25,26]. We first determined that DiE-GSSG could also be used as a substrate for recombinant PDIA3 (rPDIA3) (Fig. 2A). Using this assay, we found that 16F16 had minimal effect on the activity of rPDIA3, while both PACMA31 and CCF 642 showed inhibitory effects only at high concentrations ($\geq$100 μM) (data not shown). However, reversible inhibitor LOC14 (Fig. 2B) exhibited inhibition of rPDIA3 with an inhibitory capacity at 50% (IC50) of 4.97 μM (Fig. 2C and D).

It has been previously shown that PDIA3 is required for IAV propagation [17]. We therefore next examined, if pharmacological PDI inhibition would alter IAV propagation. We treated primary mouse tracheal epithelial cells (MTECs) with LOC14 or vehicle control (VC) prior to IAV infection, during infection, and post infection (Fig. 2E), to avoid excessive load of inhibitors and cytotoxicity at a given time. Examination of the cells 24 h post infection via flow cytometry for the presence of influenza nucleoprotein (NP) [27] (Fig. 2F), detected no NP in the mock virus infected VC or 300 μM LOC14 treated cells. IAV infected VC group showed an increase in NP and we observed a dose dependent decrease in the NP+ cells following LOC14 treatment (Fig. 2F). Using these data we were able to calculate an effective concentration 50% (EC50) of 9.952 μM for LOC14 based on the percentage of NP+ cells (Fig. 2G).

To determine if LOC14 treatment altered PDI activity within the cell we monitored the reduction of DiE-GSSG by lysates from IAV-infected cells treated with either LOC14 or vehicle control. We found LOC14 treatment (Fig. 2E), with repeated doses of 10 μM (total 30 μM), decreased PDI activity in infected MTECs compared to controls (Fig. 2H). DiE-GSSG is reported to be a substrate for PDIs [26]. Taken together these results indicate that LOC14 inhibits the oxidoreductase activity of PDIA3 and LOC14 can be used to block viral replication.

2.3. LOC14 treatment in primary mouse tracheal epithelial cells (MTECs) alters disulfide (-S-S-) bonds of HA

Influenza-HA is synthesized as a 70 kDa (HA0) precursor that is cleaved in the Golgi to yield two fragments of approximately 50 kDa (HA1) and 20 kDa (HA2) following oligomerization [28]. To determine if LOC14 alters -S-S- of HA, we treated primary MTECs with LOC14 (Fig. 3A). Briefly, MTECs were treated with 10 μM LOC14 prior to IAV infection, during infection, and post IAV infection; resulting in a total of 30 μM LOC14. Western blot (WB) analysis showed that LOC14 treatment cause no alterations in HA0 levels compared to vehicle treated cells in IAV-infected MTECs (Fig. 3B, WCL). However, levels of cleaved HA1 showed a significant decrease following LOC14 treatment (Fig. 3B, WCL-WB, Fig S2A). PDIA3 is unique compared to other PDIs in that it predominantly facilitates -S-S- bonds in glycoproteins that are being processed and traversing through the ER [29]. Therefore, we next determined whether inhibition of PDIA3 would alter -S-S- bonds of HA. We used a biotin switch assay to assess disulfides by blocking free cysteine sulfhydryl (-SH) groups using N-ethyl maleimide (NEM) and reducing -S-S- bonds with DTT, and then newly revealed -SH groups are labeled with biotin-conjugated alkylating agent (MPB) (Fig. 3C). This technique reveals high labeling of proteins with -S-S- bonds and low labeling of proteins with -SH groups. Subsequent neutravidin pull-down and Western blot analysis showed drastic decrease in -S-S- bond formation in IAV-HA following LOC14 treatment compared to vehicle control treated cells infected with IAV (Fig. 3D). We then examined

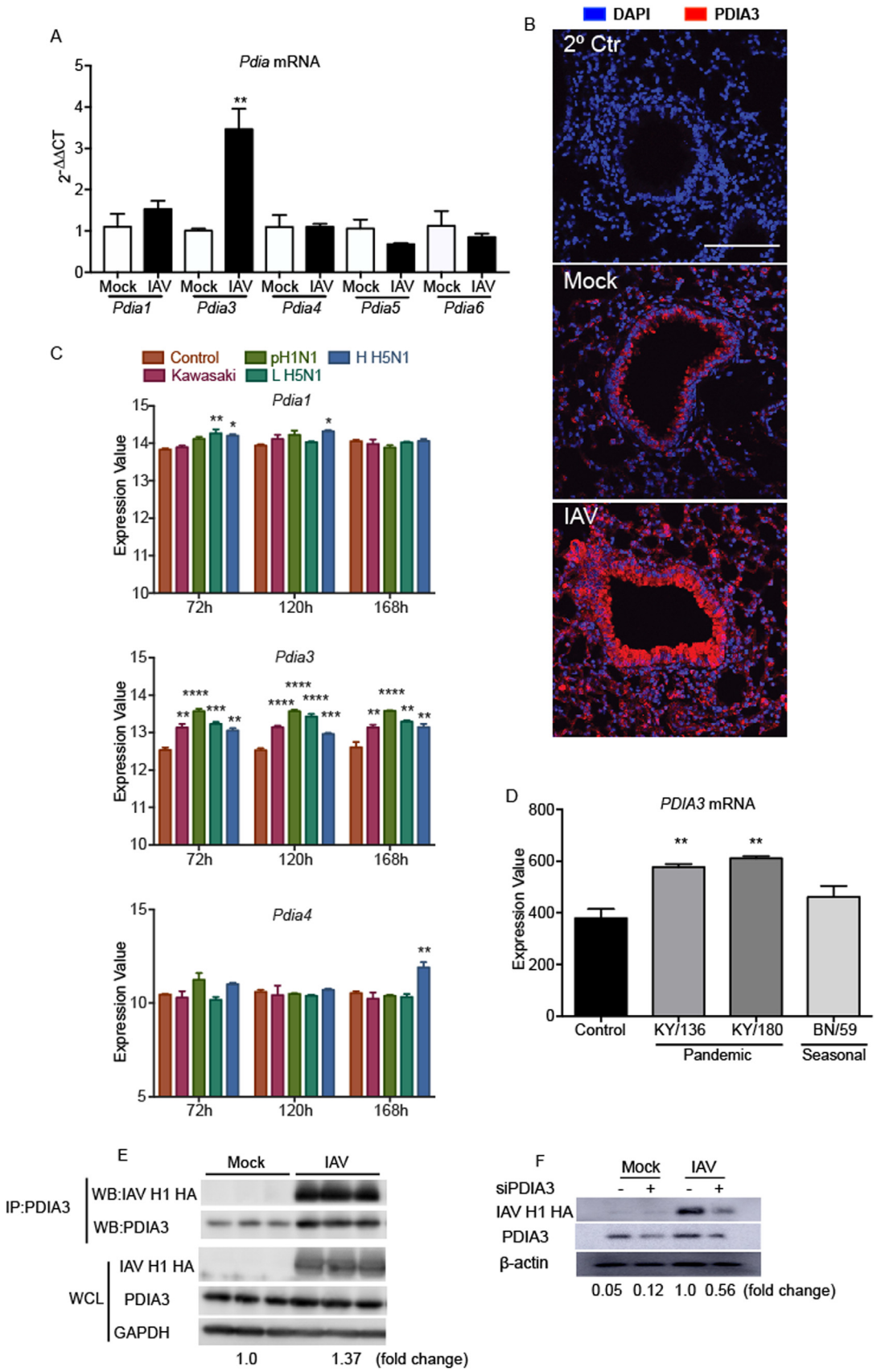

(caption on next page)

Fig. 1. PDIA3 expression is increased following IAV infection. A. Mice were infected intranasally with 2000 EIU of IAV or mock virus. *Pdia* mRNA levels were measured in whole lung lysates 6 days post infection (n = 4–5 mice/group). B. Confocal immunofluorescence microscopy of mouse lung tissue sections 6 days post infection with either IAV or mock virus stained with anti-PDIA3 antibody followed by secondary antibody conjugated to Alexa 647. Nuclei were stained with DAPI. C. Retrospective analysis of microarray data of *Pdia1*, *3*, and *4* mRNA transcript levels (GEO data set GSE63786) Data expressed as Log_2 normalized counts. D. Retrospective analysis of microarray data of *PDIA3* mRNA transcript levels from (GEO data set GSE48466). Data expressed as Log_2 normalized counts, Data are expressed as means (± SEM) * $p < 0.05$, ** $p < 0.01$, *** $p < 0.001$, *** * $p < 0.001$ by ANOVA. E. Western blot analysis of IAV HA: PDIA3 interaction in HBE cells following PDIA3 immunoprecipitation. Numbers below indicate average densitometry per group of WCL PDIA3 normalized to GAPDH F. Western blot analysis of IAV HA and PDIA3 in mouse lung epithelial cells transfected with scrambled (-) or *Pdia3*-specific siRNA (+). Numbers below indicate densitometry of IAV HA normalized to β actin.

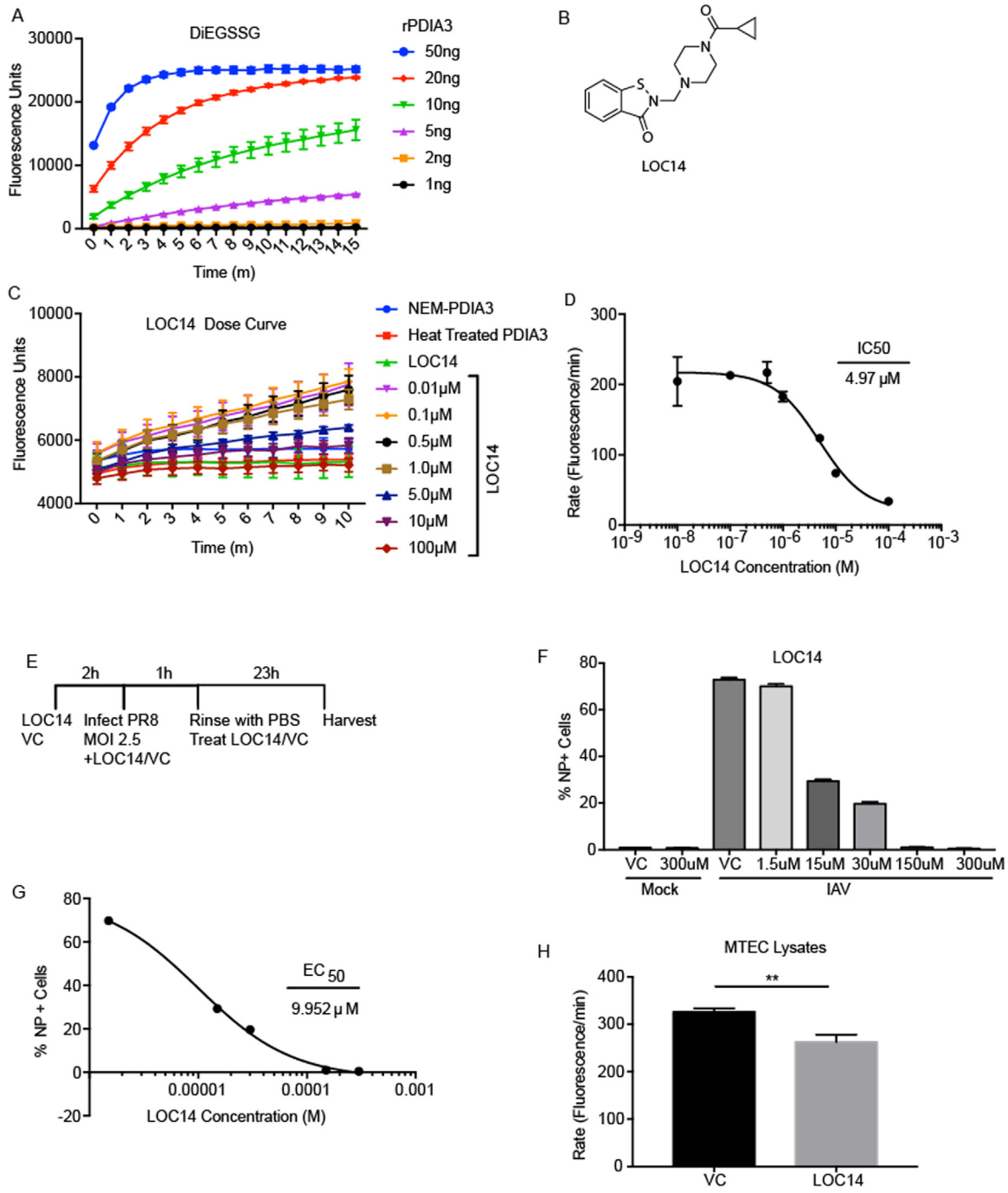

Fig. 2. PDI inhibitor LOC14 inhibits PDIA3 and decreases influenza protein production. A. Kinetics of PDIA3 catalyzed reduction of DiE-GSSG in the presence of increasing concentrations of recombinant PDIA3. B. Chemical structure of reversible PDI inhibitor LOC14. C. Dose dependent inhibition of PDIA3 reductase activity with LOC14. Heat-treated rPDIA3, alkylated (NEM) rPDIA3, and LOC14 without PDIA3 were included as controls. D. IC50 of LOC14 for PDIA3 determined based on the initial rate of fluorescence formation from C. E. Treatment regimen for LOC14 in MTEC cells. F. Percentage of IAV NP + primary mouse tracheal epithelial cells 24 h post infection with IAV or mock virus following treatment with LOC14 or vehicle control. G. EC50 of LOC14 determined from percentage of infected cells from F. H. Significant decreases in PDI activity in the cells treated with LOC14. * * $p < 0.01$ by *t*-test.

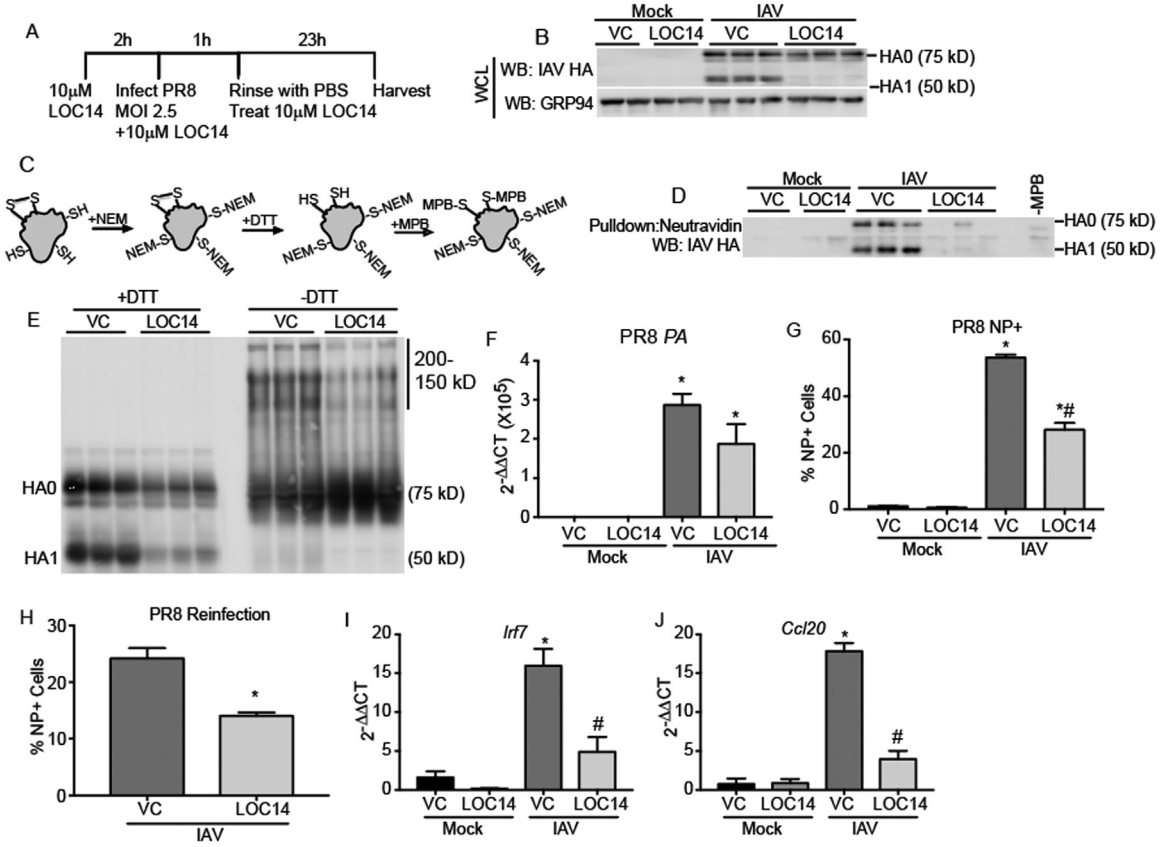

Fig. 3. LOC14 treatment in primary mouse tracheal epithelial cells (MTECs) decreases -S-S- of HA and viral burden. A. Schematic representing the time points of IAV infection and LOC14 treatment. B. Western blot analysis of PR8 HA0/HA1 of cells treated as in A. GRP94 was used as a loading control. Duplicates (mock) and triplicates (IAV) of identical conditions are shown. C. Schematic depicting biotin switch assay and subsequent labeling of reduced sulfhydryl groups by MPB. D. Western blot analysis of thiol content of IAV HA following LOC14 treatment by MPB labeling and neutravidin pulldown. E. Western blot analysis of HA oligomerization following LOC14 treatment of IAV infected cells, samples analyzed by reducing (+DTT) and non-reducing (-DTT) run on a SDS-PAGE. F. mRNA expression of IAV *PA* from cell lysates of mock infected and IAV infected primary MTECs analyzed by RT-qPCR. G. Percentage of IAV NP+ MTECs following LOC14 treatment, *p < 0.05 compared to mock groups, #p < 0.05 compared to IAV-VC group by ANOVA. H. Percentage of IAV NP+ MTECs following exposure to LOC14 or vehicle control treated supernatant from F, *p < 0.05 compared to VC group by *t*-test. I and J. mRNA expression of *Irf7* and *Ccl20* from cell lysates of mock infected and IAV infected primary MTECs analyzed by RT-qPCR. PCR results were normalized to housekeeping gene *Gapdh*. *p < 0.05 compared to mock groups, #p < 0.05 compared to IAV-VC group by ANOVA. Data are expressed as means (± SEM) of 3 samples per group.

oligomerization of HA using non-reducing SDS-PAGE. Mature HA trimers are known to be resistant to dissociation by SDS [30,31]. LOC14 treatment increased monomeric HA and correspondingly decreased high molecular weight HA (150–200 kDa) as compared to vehicle treated controls (Fig. 3E, right lanes, -DTT). Samples reduced using DTT showed no high molecular weight HA (Fig. 3E, left lanes, +DTT). Indicating LOC14 induces defects in HA oligomerization by altering oxidative folding of HA. Interestingly, we observed a small decrease in monomeric forms of HA0 and a marked decrease of HA1 in LOC14 treated samples compared to vehicle control samples infected with IAV (Fig. 3E, left lanes, +DTT). Potentially suggesting a decrease in overall HA production following LOC14 treatment.

Our analysis of IAV burden in these cells showed a decrease in IAV-*PA* transcripts following LOC14 treatment, but this was not statistically significant (Fig. 3F). However we observed a significant decrease in the number of MTECs positive for IAV NP in LOC14 treated IAV infected cells as compared to vehicle control treated cells (Fig. 3G & S2B). Next, reinfection of MTECs with supernatants isolated from earlier infected MTECs treated with either vehicle or LOC14 showed a marked decrease in the number of cells positive for IAV NP in LOC14 treated supernatants as compared to vehicle treated supernatants (Fig. 3H & S2C), suggesting a decreased production of infectious virus following LOC14 treatment. Quantification of mRNAs for *Ccl20*, and *Irf7*, an important transcriptional regulator of the type I interferon response by RT-qPCR showed a significant decrease in transcript levels following LOC14 treatment, suggesting decreased viral burden (Fig. 3I & J).

LOC14 is known to be a potent activator of the unfolded protein response (UPR)[23]. In order to assess UPR due to LOC14 treatment, we examined UPR activation, by monitoring ATF6 cleavage and GRP78 protein expression, two transducers of the UPR, and measurement of active caspase-3. Our results showed no significant increases in either readout in LOC14 treated samples, indicating LOC14 (30 μM) treatment had no effect on cellular stress levels of either mock or IAV infected cells 24 h post infection (Fig S2D & S2E).

Taken together these results suggest that LOC14 alters oxidative folding of HA, and that deficit in the formation of disulfide bonds has significant implications for oligomerization of HA and subsequent influenza burden in MTECs.

2.4. LOC14 treatment alters oxidative folding of different HA in H3N2 serotype

Owing to remarkable conservation of cysteine residues between various strains of influenza (Fig S3) we sought to determine if alterations in oxidative folding also affected other hemagglutinin serotypes e.g. H3. To determine the effects of LOC14 treatment on H3 HA, we infected MTECs with X31 which contains the HA and NA genes of A/Aichi/1/1968 (H3N2) [32]. Primary MTECs were treated with LOC14

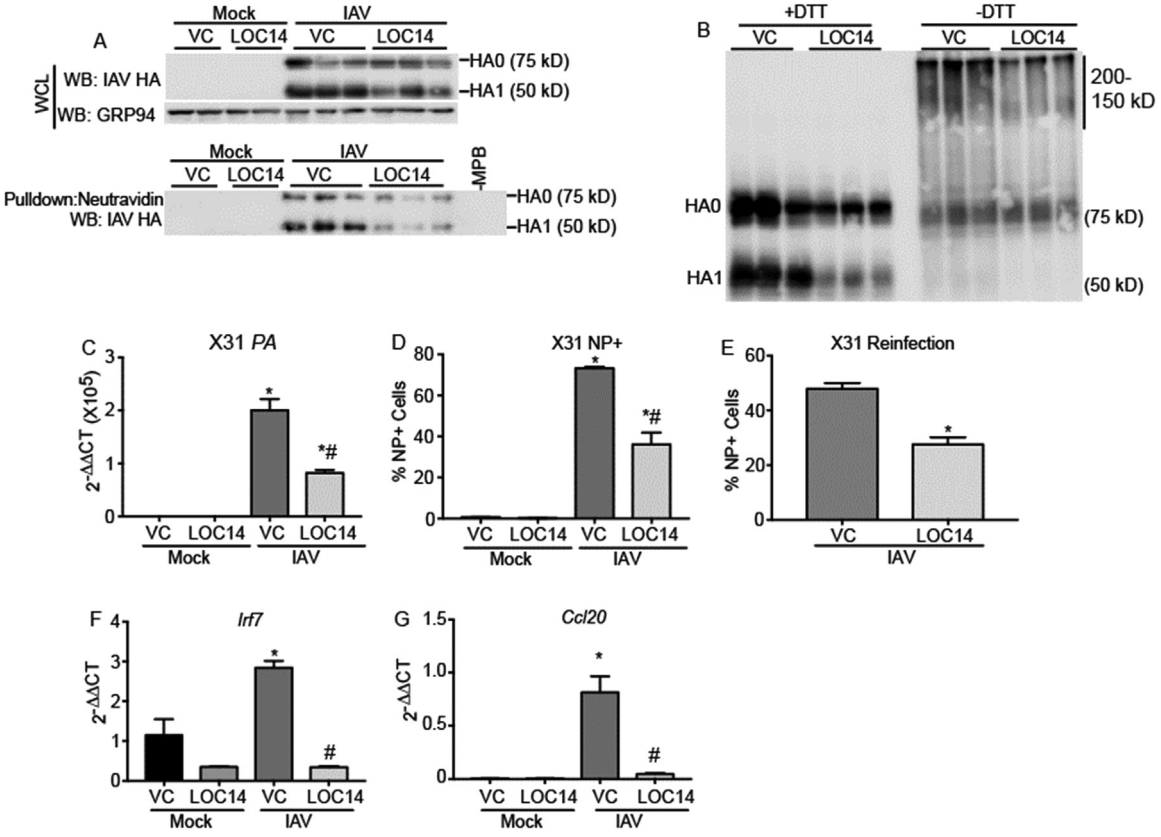

Fig. 4. LOC14 treatment alters oxidative folding of different HA in H3N2 serotype. A. Western blot analysis of X31 HA0/HA1, GAPDH was used as a loading control (top panel), Western blot analysis of thiol content of IAV HA following LOC14 treatment by MPB labeling and neutravidin pulldown (bottom panel). B. Western blot analysis of HA oligomerization following LOC14 treatment of IAV infected cells, samples analyzed by reducing (+DTT) and non-reducing (-DTT) run on a SDS-PAGE. C. mRNA expression of IAV *PA* from cell lysates of mock infected and IAV infected primary MTECs analyzed by RT-qPCR, *p < 0.05 compared to mock groups, #p < 0.05 compared to IAV-VC group by ANOVA. D. Percentage of IAV NP+ MTECs following LOC14 treatment by flow cytometry, *p < 0.05 compared to mock groups, #p < 0.05 compared to IAV-VC group by ANOVA. E. Percentage of IAV NP+ MTECs following exposure to LOC14 or vehicle control treated supernatant from E by flow cytometry, *p < 0.05 compared to VC group by *t*-test. F and G. mRNA expression of *Irf7* and *Ccl20* from cell lysates of mock infected and IAV infected primary MTECs analyzed by RT-qPCR. PCR results were normalized to housekeeping gene *Gapdh*. *p < 0.05 compared to mock groups, #p < 0.05 compared to IAV-VC group by ANOVA. Data are expressed as means (± SEM) of 3 samples per group.

pre- and post-infection with X31 (Fig. 3A). LOC14 treatment did not alter HA0 levels compared to vehicle treated cells (Fig. 4A, WCL-WB). However, levels of cleaved HA1 showed a significant decrease following LOC14 treatment (Fig. 4A, WCL-WB, top panel, Fig S4A). The biotin switch assay followed by neutravidin pull-down showed considerably less disulfide bonds in IAV-HA (H3) following LOC14 treatment (Fig. 4A, neutravidin-WB, bottom panel). We then examined oligomerization of HA using non-reducing SDS-PAGE. LOC14 treatment decreased high molecular weight HA (150–200 kDa) as compared to vehicle treated controls (Fig. 4B, right lanes, -DTT), while samples reduced using DTT showed no high molecular weight HA (Fig. 4B, left lanes, +DTT), though no corresponding increase in monomeric HA was observed. These results suggest that a decrease in oxidative folding in the form of -S-S- bonds of HA leads to impaired oligomerization in H3-HA of X31. Again, we observed a decrease in monomeric forms of HA0 in LOC14 treated samples compared to vehicle control samples infected with IAV (Fig. 4B, left lanes, +DTT). Potentially suggesting that a decrease in overall HA production following LOC14 treatment.

Subsequent analysis of IAV burden in these cells showed a significant decrease in IAV-*PA* transcripts following LOC14 treatment (Fig. 4C), and a significant decrease in the number of MTECs positive for IAV-NP in LOC14 treated IAV infected cells as compared to IAV infected vehicle control treated cells (Fig. 4D, S4B). Next, reinfection of MTECs with supernatants isolated from earlier infected MTECs treated with either vehicle or LOC14 showed a marked decrease in the number of cells positive for IAV NP, suggesting decreased production of infectious virus following LOC14 treatment (Fig. 4E, S4C). Quantification of *Ccl20*, and *Irf7*, by RT-qPCR showed a significant decrease in transcript levels following LOC14 treatment (Fig. 4F and G). Taken together these results suggest that LOC14 decreases -S-S- bonds of H1 as well as H3 HA, and that these variations in disulfide bonds have significant implications for oligomerization of HA and subsequent inflammatory response independent of influenza strain.

2.5. Ablation of Pdia3 in the lung epithelium attenuates viral burden in mice

To determine whether PDIA3 in airway epithelial cells contributes to the establishment of viral burden, lung inflammation and airway mechanics, we generated a doxycycline inducible transgenic *CCSP-rTetA/TetOP-Cre/Pdia3*$^{loxp/loxp}$ (Δ*Epi-Pdia3*) mouse to delete *Pdia3* specifically in lung epithelial cells. Mice carrying *TetOP-Cre/Pdia3*$^{loxp/loxp}$ or *CCSP-rTetA/TetOP-Cre* were used as littermate controls (*Ctr*). Characterizations of these mice are described elsewhere [6]. All mice were kept on doxycycline for the length of the experiment beginning seven days prior to IAV infection to ensure ablation of *Pdia3* throughout the infection protocol (Fig. 5A). Our previous work with these transgenic mice show clear decrease of PDIA3 following doxycycline exposure in the lung epithelial cells [6]. RT-qPCR analysis of viral transcripts (IAV-*PA*, *-HA*, and *–NA*) in lung extracts showed significantly decreased viral load as evidenced from the influenza markers that are examined in Δ*Epi-Pdia3* mice compared to *Ctr* mice (Fig. 5B-D). Strikingly, Western blots showed that HA protein levels were significantly

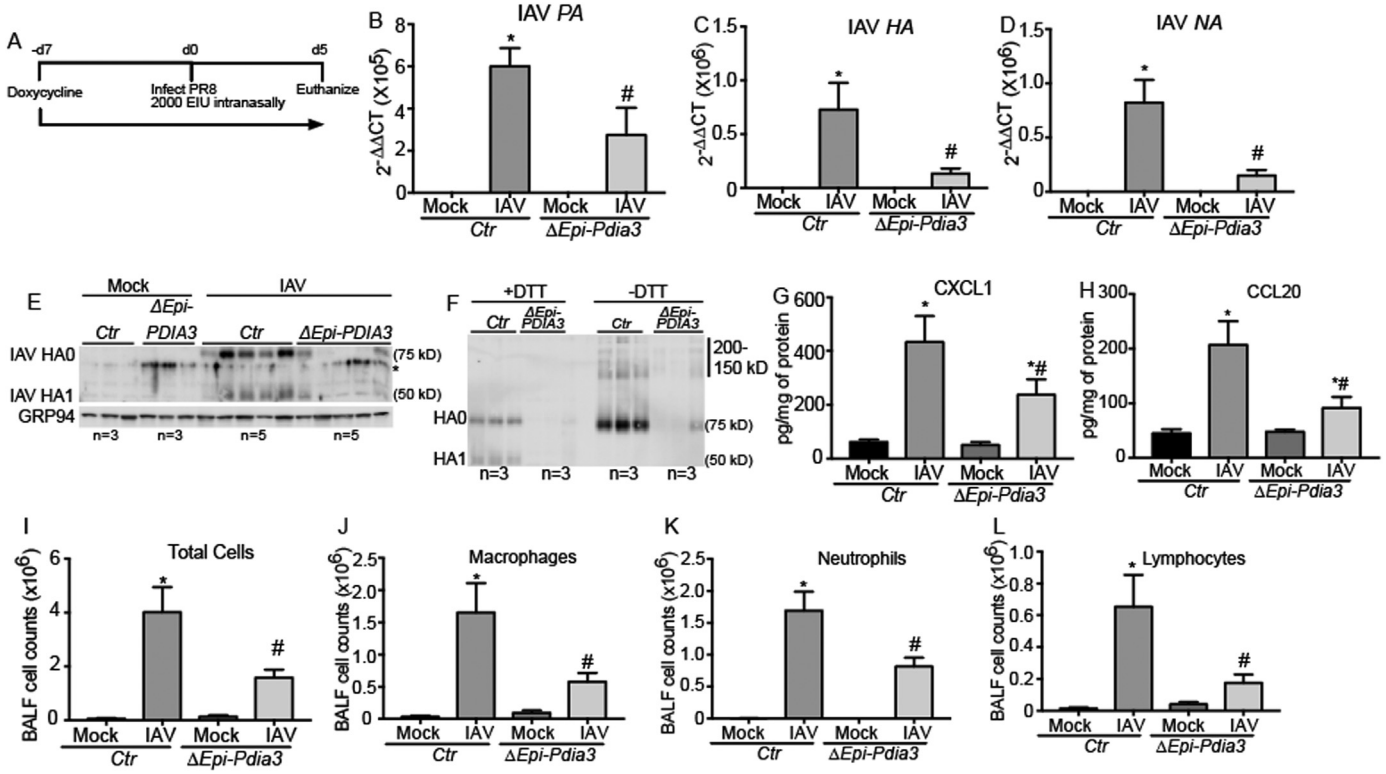

Fig. 5. Ablation of *Pdia3* in the lung epithelium attenuates viral burden and inflammation in mice. A. Schematic representing the time points of IAV infection and doxycycline treatment and euthanasia of mice. B-D. Analysis of mRNA for influenza proteins (*PA*, *HA* and *NA*) in whole lung lysate by RT-qPCR, results normalized to the geometric mean of housekeeping genes *Pp1b* and *Gapdh*, *p < 0.05 compared to mock groups, #p < 0.05 compared to IAV-*Ctr* group by ANOVA. E. Western blot analysis of IAV HA in *Ctr* and Δ*Epi-Pdia3* mice, GRP94 was used as a loading control. * Indicates nonspecific band. F. Western blot analysis of HA oligomerization following ablation of PDIA3 in the airway epithelium, samples analyzed by reducing (+DTT) and non-reducing (-DTT) SDS-PAGE. G and H. ELISA for CXCL1 and CCL20 from whole lung homogenates, *p < 0.05 compared to mock groups, #p < 0.05 compared to IAV-*Ctr* group by ANOVA. I-L. Analysis of inflammatory and immune cells in the BALF by hema 3 stain and differential counting, *p < 0.05 compared to mock groups, #p < 0.05 compared to IAV-*Ctr* group by ANOVA. Data are expressed as means (± SEM) of 6–10 mice/group.

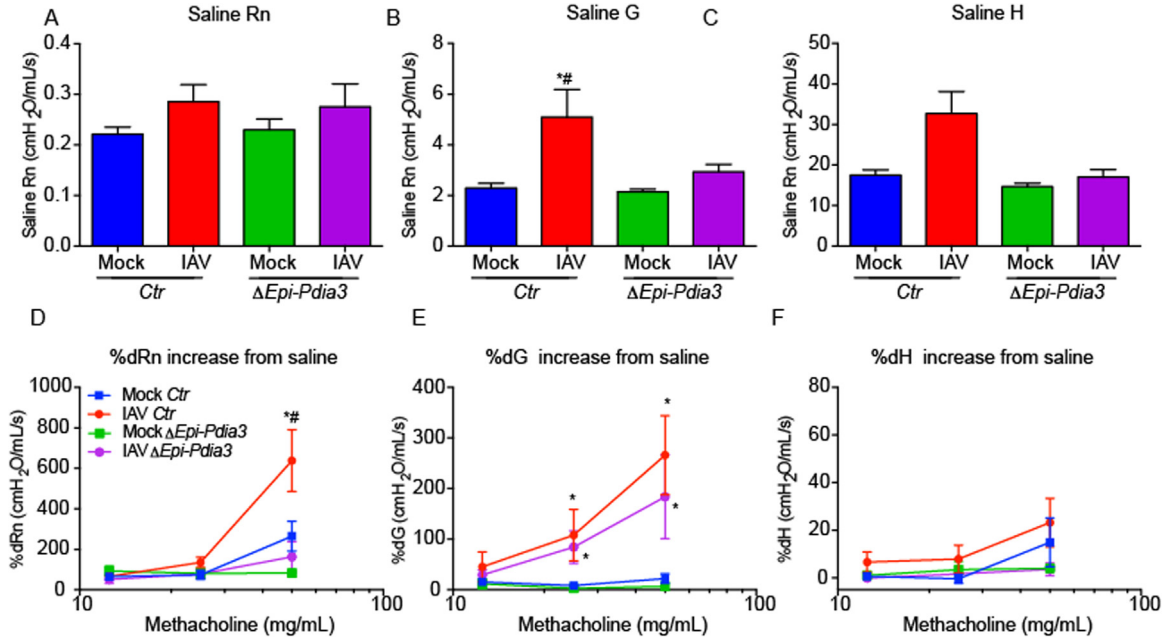

Fig. 6. Ablation of *Pdia3* in the lung epithelium attenuates influenza-mediated methacholine induced AHR. A-C. Assessment of AHR via a forced oscillation technique in *Ctr* and Δ*Epi-Pdia3* mice. Saline was administered to determine baseline Newtonian resistance (Rn), tissue resistance (G), and tissue elastance (H), *p < 0.05 compared to mock groups, #p < 0.05 compared to IAV-Δ*Epi-Pdia3* group by ANOVA. D-F. Methacholine (12.5–50 mg/mL) induced AHR represented as percent increase from saline following exposure to increasing doses of methacholine. *p < 0.05 compared to mock groups, #p < 0.05 compared to IAV-Δ*Epi-Pdia3* group by ANOVA. Data are expressed as means (± SEM) of 6–10 mice/group.

decreased following lung epithelial *Pdia3* ablation (Fig. 5E, Fig S5). Accordingly, these decreases in HA also resulted in decreased HA oligomers (150–200 kDa) in- Δ*Epi-Pdia3* mice compared to *Ctr* mice (Fig. 5F). Taken together these results suggest lung epithelial PDIA3 plays an important role in efficient HA production and IAV burden *in vivo*.

We next determined if this decrease in viral burden due to *Pdia3* deletion led to a concomitant decrease in influenza-induced inflammation. Analysis of chemokines in the lung tissues showed that production of neutrophil chemoattractant CXCL1 and dendritic/macrophage chemoattractant CCL20 were decreased in IAV-infected Δ*Epi-Pdia3* mice when compared with IAV-infected *Ctr* mice. (Fig. 5G and H). Analysis of total cells in bronchoalveolar lavage fluid (BALF) also showed a significant decrease in inflammatory cell numbers in Δ*Epi-Pdia3* mice infected with IAV as compared to *Ctr* mice infected with IAV (Fig. 5I). Quantitation of specific inflammatory cell types revealed significant attenuation of total macrophages, neutrophils, and lymphocytes in IAV infected Δ*Epi-Pdia3* mice when compared with IAV infected *Ctr* mice (Fig. 5J-L).

2.6. Ablation of Pdia3 in the lung epithelium attenuates influenza-induced airway hyperresponsiveness (AHR)

Viral infection is known to increase methacholine sensitivity and AHR in mice and humans [33–35]. Therefore, we examined the consequence of epithelial specific deletion of *Pdia3* on AHR to increasing doses of inhaled methacholine. Following the saline (vehicle control for methacholine) challenge, peripheral airway resistance (G), but not central airway resistance (Rn) or parenchymal tissue elasticity (H), was elevated in control (C*tr*) mice infected with IAV compared to mock infected *Ctr* mice, suggesting that IAV caused dysfunction of the small airways and/or lung parenchyma [36] (Fig. 6A-C). However, there was no increase in G in Δ*Epi-Pdia3* mice infected with IAV. Furthermore, methacholine challenges showed that IAV increased AHR as measured by changes in both Rn and G; however the severity of the AHR measured by both G and Rn was significantly decreased in IAV-infected Δ*Epi-Pdia3* mice (Fig. 6D & E). This suggests that due to IAV infection, the presence of PDIA3 increases responsiveness to methacholine and results in constriction of the central and peripheral airways. Taken together these results suggest that lung epithelial PDIA3 plays an important role in the establishment of IAV burden, inflammation, and AHR

3. Discussion

The pathogenesis of IAV involves a complex interplay between numerous host and viral factors [37]. Additional understanding of the influenza virus as well as the host cellular pathways utilized by IAV would provide valuable insight toward the development of novel therapeutic and preventative modalities less dependent on viral antigenic shift and drift.

Recent studies have suggested that several PDIs play important roles in influenza pathogenesis [17,38]. However only the calnexin/calreticulin associated, glycoprotein specific PDIA3 is known to be directly involved in the processing of IAV hemagglutinin (HA), one of the major antigenic determinants of the virus [15,17,39]. Disrupting this PDIA3-HA interaction provides an intriguing therapeutic target. While there is a large amount of diversity in IAV hemagglutinin [40], the cysteine residues involved in disulfide bonding are highly conserved (Fig S3), highlighting their importance in the structure and function of HA.

Herein, we show that PDIA3 levels are increased following IAV infection, and PDIA3 transcript levels are upregulated compared with other PDIs. Treatment with a reversible PDI inhibitor LOC14 results in altered -S-S- bonds in both H1 and H3 HA along with associated alterations of HA maturation and subsequent decreases in markers of viral infection, demonstrating potent anti-influenza activity independent of viral strain. While LOC14 is known to be a potent UPR activator [23], 24 h post LOC14 treatment the cells do not show signs of exacerbated cellular stress or enhanced apoptosis. Furthermore, genetic ablation of *Pdia3* in the airway epithelium, the primary site of influenza infection, results in a similar phenotype of diminished overall viral load. Finally we also show restoration of normal lung mechanics following *Pdia3* ablation in IAV infected mice. Taken together our results suggest the importance of lung epithelial PDIA3 in formation of -S-S- bonds of IAV HA and subsequent establishment of IAV infection, airway inflammation and AHR.

PDIs play critical roles in oxidative folding of proteins, catalyzing and isomerizing disulfide bonds [7]. PDIA3 is required for the efficient folding of HA by catalyzing and isomerizing disulfide bonds and ensuring proper cysteine pairings [15]. Past work has demonstrated the necessity of these disulfides in the proper folding of HA, as well as in the formation of the HA trimer and its transport through the secretory system of the cell to the plasma membrane [14,41], potentially linking oxidative folding to viral assembly. LOC14 treatment led to significant alterations of the disulfide bonds of both H1 and H3 HA. Regardless of IAV strain, HA cleavage occurs after it has left the ER, either in the Golgi or at the cell surface [42,43]. Following LOC14 treatment we observe a marked decrease in HA1, which suggests that altered oxidative folding prevents the normal proteolytic processing of HA. Studies involving HA mutants lacking the ability to form proper disulfide bonds demonstrate retention of the mutant misfolded HA in the ER and enhanced proteasome-mediated degradation [14,44–47].

HA is known to oligomerize to its SDS resistant trimeric conformation within the ER regardless of ATP concentration, blocked transport from the ER, temperature alterations, and the trimming of carbohydrate side chains [31]. This suggests that trimerization is largely dependent on the acquisition of the proper tertiary structure of the HA0 monomers. Impairment of proper disulfide bond formation has been shown to hinder detection of correctly folded trimeric HA; moreover, *Pdia3* deletion has shown to cause a decreased number of HA molecules acquiring its trimeric structure [14,15]. We found that PDI inhibition with LOC14 resulted in a similar phenotype, causing a marked decrease in the appearance of high molecular weight SDS resistant HA species combined with concomitant increases in monomeric H1-HA, though no increase in monomeric H3-HA was observed. Collectively, these results suggest that alteration in HA maturation (oligomerization) is driven by intramolecular -S-S- bonds rather than other protein modifications.

Interestingly we observe variable decreases in HA0 levels following LOC14 treatment for both H1-HA and H3-HA on Western blots. These variations may be due to differences in the amount of protein used as well as different gel-running time for the various Western blots.

While LOC14 treatment has an effect on the folding of HA, at this juncture, it is not possible to determine which PDIs are being affected. LOC14 has been extensively characterized against PDIA1, the prototypical member of the PDI family. It has been proposed in the literature that LOC14 would be effective against other PDI family members owing to high sequence homology and conservation of the active site, though this has yet to be verified [18,22]. siRNA experiments have shown PDIA1, 3, and 4 all play some role in influenza infection, leading to significant decreases in viral replication, though no viral proteins that reach the plasma membrane through the secretory pathway were examined [38]. Thus the effects we see could be the result of LOC14 inhibiting multiple PDIs, though PDIA3 is the only PDI directly involved in HA maturation [15]. However a lack of specificity would theoretically result in substantial loss of PDI activity in cell lysates treated with LOC14; while we observe significant decreases in PDI activity there is nonetheless high background signal in lysates of cells treated with LOC14. This could suggest that DiE-GSSG might be able to act as a substrate for other redox active cellular proteins such as thioredoxins or glutaredoxins. Another possibility is an alteration of the equilibrium between the bound and unbound inhibitor, the inhibitory capacity of

LOC14 may be altered under diluted assay conditions. Further refinement and experimentation are needed to accurately assess the biological capacity of LOC14 on PDI activity in influenza-infected cells.

LOC14's lack of specificity toward a single PDI may also explain differences in chemokine levels following treatment. Various PDIs might be involved more directly in not only the production, but also the secretion of these chemokines or other cytokines, for example, PDIA1 is found at high levels in the secretory granules of eosinophils [48], and we have previously shown siRNA knockdown or ablation of *Pdia3* in lung epithelial cells decreases various cytokine levels, and alters oxidative folding of Eotaxin, EGF and Periostin in mice [6].

The lack of specificity of LOC14 also leaves open the possibility of inhibiting not only PDIs but also other oxidoreductaes with thiredoxin fold [18,49]. Thioredoxin reductases utilize selenocysteine to mediate their effects [50], as such the potential interactions with LOC14 are harder to predict. Direct interaction between these proteins and viral HA is unlikely, as they are not found in high abundance within the ER [49,50]. Previous work has demonstrated treatment with glutathione derivatives significantly decreases influenza replication, which was attributed to an alteration in the redox state of PDIs [51], suggesting the importance of the redox buffering capacity of the cell for influenza replication. We predict that if LOC14 is able to interact with these redox-buffering enzymes it would allow for the possibility of additional indirect inhibition of PDIs, though extensive experimentation would be required to accurately determine additional LOC14 targets.

To investigate the role of PDIA3 during IAV infection *in vivo* we deleted *Pdia3* specifically in the lung epithelium. Our results show deletion of *Pdia3* in the lung epithelium significantly decreased overall viral load. Moreover we show *Pdia3* deletion significantly attenuates IAV mediated airway inflammation and AHR. *Pdia3* deletion strikingly ablates increases in peripheral airway resistance found in control mice following IAV infection. Viral infection is known to induce or exacerbate AHR in humans and mice [33,34], and present data provides strong evidence that deletion of PDIA3 in the lung epithelium leads to relevant improvements of lung mechanics. The protection against changes in Rn and G during methacholine challenge suggest the changes are due to reduced airway narrowing of both large and small airways [52,53]. While the lack of effect on H suggests that is does not change the severity of airway closure during methacholine challenge [54]. Though it remains possible the reduction in AHR is simply due to decrease in viral burden following ablation of *Pdia3*.

Interestingly HA levels were severely decreased after ablation of PDIA3, pointing to a potential role for PDIA3 in influenza entry into the cell. In certain cells PDIA3 found on the plasma membrane is known to play an important role in gamete fusion, act as a receptor for certain vitamins, and facilitate HIV entry [55–57]. However experiments using cell impermeable PDI inhibitors showed little impact on influenza replication, suggesting PDIA3's role in influenza propagation may be limited to protein maturation in the ER [38].

In conclusion, our findings support that PDIA3 activity is involved in IAV replication, specifically in the oxidative folding of IAV HA. Interestingly this effect appears to occur independent of influenza strain. Lung epithelial specific ablation of *Pdia3* suggested that IAV infection and spread may require *Pdia3 in vivo* and ablation of *Pdia3* also decreased inflammatory markers as well as virus load in the lung. These results suggest that inhibiting PDIA3 during influenza infection may decrease viral load and improve lung mechanics. Furthermore, we have shown that a reversible, small molecule PDI inhibitor LOC14 has anti-influenza activity and may form a potential basis for future anti influenza therapeutics by inhibiting PDIs.

4. Material and methods

4.1. Ethics statement

All animal studies were approved by the University of Vermont Institutional Animal Care and Use Committee and carried out in accordance with the Guide for the Care and Use of Animals of the National Institutes of Health. The University of Vermont adheres to the "U.S. Government Principles for the Utilization and Care of Vertebrate Animals Used in Testing, Research, and Training", "PHS Policy on Humane Care and Use of Laboratory Animals", "USDA: Animal Welfare Act & Regulations", and "the Guide for the Care and Use of Laboratory Animals". The University is accredited by the Association for Assessment and Accreditation of Laboratory Animal Care International (AAALAC). University of Vermont's PHS Assurance Number: A3301-01, expiration date: October 31, 2021. University of Vermont IACUC was approved on July 30, 2013, and the animal protocol number is 13–063. The de novo renewal was approved on July 17, 2018, and the animal protocol number is 13–063.

4.2. Viruses

Influenza A virus Puerto Rico 8/34 (H1N1) (10100374) and A X-31, A/Aichi/68 (H3N2) (10100375) were purchased from Charles River.

4.3. Cells and treatments

Primary MTECs were isolated and cultured from age and sex matched wild type (WT) C57BL/6NJ mice as previously described [6]. Cells were plated at 2×10^6 cells/dish and when greater than 90% confluent, infected with mouse-adapted H1N1 influenza A virus Puerto Rico 8/34 (PR8) or H3N2 A X-31, A/Aichi/68 (X31) at 2.5 Egg infectious units (EIU)/cell in a DMEM/F12 (Gibco) growth factor–free medium. Ultraviolet light (UV)–irradiated virus that was replication-deficient (mock) was used as a control. Following infection the cells were incubated for 1 h at 37 °C, the plates were then washed twice with 2 mL PBS to remove unbound virus, and supplemented with growth factor–free medium. MTECs were pretreated for 2 h with 10 μM LOC14 (Tocris, 5606), during viral infection, and 1 h post viral infection, DMSO was used as a control. All treatments were performed in growth factor–free medium.

4.4. Transgenic mice

Bitransgenic mice carrying the rat club cell secretory protein (CCSP) promoter 5′ to the open reading frame for the reverse tetracycline transactivator (*CCSP-rtTA*; line 1, which in adult lungs is expressed in bronchiolar and type II epithelial cells) [58] plus 7 tetracycline operon 5′ to the open reading frame for Cre recombinase *(TetOP-Cre)* mice were provided by Dr. Whitsett (Cincinnati Children's Hospital) [59]. *CCSP-rtTA*$^+$, *TetOP-Cre*$^+$ mice were bred with mice carrying the *Pdia3*$^{loxp/loxp}$ alleles [60]. Mice expressing *CCSP-rtTA/TetOP-Cre/Pdia3*$^{loxp/loxp}$ were used to ablate Pdia3 from lung epithelial cells (denoted as Δ*Epi-Pdia3*) by feeding doxycycline-containing chow (6 g/kg; Purina Diet Tech, St Louis, Mo) 7 days before exposure to virus. Mice were maintained on doxycycline-containing food until completion of the experiment. Double-transgenic littermates containing either *CCSP-rtTA/TetOP-Cre* or *CCSP-rtTA/Pdia3*$^{loxp/loxp}$ (*Ctr* mice) and fed doxycycline-containing food were used as controls in the experiments.

4.5. Assessment of AHR

Mice were anesthetized by IP injection of pentobarbital solution (90 mg/kg), tracheotomized with an 18 gauge cannula, then mechanically ventilated at a rate of 200 breaths/min using a FlexiVent computer controlled small animal ventilator (SCIREQ). While on ventilators mice

received the paralytic, pancuronium bromide. Parameters of Newtonian resistance (Rn), tissue dampening (G), and elastance (H) were calculated as previously described [61]. Airway hyperresponsiveness is represented as the average of the three peak measurements for each animal, obtained at increasing methacholine doses.

4.6. Bronchoalveolar lavage processing

Bronchoalveolar lavage fluid (BALF) was collected by lavaging lungs with 1.0 mL of sterile PBS. Cells were isolated by centrifugation, and total cell counts were determined using a hemocytometer (Hausser Scientific) on an Inverted Infinity and Phase Contrast Microscope (Fisher Scientific). Differential cell counts were obtained via cytospins using Hema3 stained (Fisher Scientific) total cells. Differentials were performed on a minimum of 300 cells/animal.

4.7. Analysis of mRNA expression

Right lung lobes were flash-frozen and pulverized, and total RNA was isolated using Qiazol Lysis Reagent (Qiagen) and purified using the RNeasy kit (Qiagen). One microgram of RNA was reverse transcribed to cDNA for quantitative assessment of gene expression using SYBR green (Bio-Rad). Expression values were normalized to indicated housekeeping gene(s). The primers used in this study are listed in Supplemental Table 1.

4.8. Western blot analysis

Following dissection, right lung lobes were flash-frozen for protein or mRNA analysis. Lungs were pulverized and lysed in buffer containing 20 mM Tris·HCl (pH 8.0), 100 mM NaCl, 0.5% Nonidet P-40, 10% glycerol, and 1% protease inhibitor cocktail (Sigma-Aldrich, P8340) (v/v), 1% phosphatase inhibitor cocktails 1 and 2 (Sigma-Aldrich, P5726, P0044) (v/v). Proteins from cell lysates were prepared in the same buffer. Insoluble proteins were pelleted via centrifugation. Following protein quantitation of the supernatant, samples were resuspended in loading buffer with dithiothrietol and resolved by SDS-PAGE. Proteins were transferred to PVDF, and membranes were probed using a standard immunoblotting protocol. Protein quantification of supernatant was determined using DC Protein Assay (Bio-Rad, 5000116). Samples were resuspended in loading buffer with dithiothrietol and resolved by SDS-PAGE. The quantification of protein expression was performed by densitometry using Image Studio Lite software (LI-COR Biosciences). Antibodies used for western blots can be found Supplemental Table 2

4.9. Image processing

Digital images were acquired using an Amersham Imager 600RGB (GE). Photoshop (CC 2018; Adobe) and Illustrator (CC 2018; Adobe) were used to assemble the figures. Samples were run on the same gel. When required, brightness and contrast were adjusted equally in all lanes.

4.10. ELISA

Lung protein samples were assayed for CXCL1 (DY453, R&D) and CCL20 (DY760, R&D) by ELISA according to the manufacturer's instructions.

4.11. Non-reducing gel electrophoresis

Lung homogenates were resuspended in loading buffer without the reducing agent dithiothrietol (DTT). A separate set of samples were resuspended in loading buffer with DTT and incubated at 95 °C for 10 min to reduce the disulfide bonds. The samples were resolved by SDS-PAGE and subjected to western blot analysis as described.

4.12. Immunofluorescence

Following euthanization, left lobes were fixed with 4% paraformaldehyde, stored at 4 °C overnight for fixation of the tissue, mounted in paraffin, and 5 μm sections were affixed to glass microscope slides for histopathology as previously described [61]. Sections were prepared for immunofluorescence by deparaffinizing with xylene and rehydrating through a series of ethanols. For antigen retrieval, slides were heated for 20 min in 95 °C pH 6.0 sodium citrate buffer with 0.05% TWEEN-20 then rinsed in dH_2O. Sections were then blocked for 1 h in 1% BSA in PBS, followed by incubation with primary antibody for PDIA3 (LSBio, LS-B9768) at 1:300, overnight at 4 °C. Slides were then washed 3 × 5 min in PBS, incubated with Alexafluor 647 at 1:1000 in 1% BSA, and counterstained with DAPI in PBS at 1:4000 for nuclear localization. Sections were imaged using a Zeiss 510-META confocal laser-scanning microscope. Images were captured at x40 magnification in oil immersion. The image files were converted to Tiff format. Brightness and contrast were adjusted equally in all images.

4.13. PDIA3 activity assay

PDI disulfide reduction activity was monitored in PDI assay buffer containing 0.1 M potassium phosphate buffer pH 7.0 and 2 mM EDTA by adding 10 ng recombinant human PDIA3 (Prospec, ENZ-474) or 2 μg MTEC lysate to 150 mM DiE-GSSG (Cayman, 11547) in the presence of 5 μM DTT. DiE-GSSG is comprised of two eosin molecules attached to oxidized glutathione, resulting in proximity quenching of the eosin molecules. Upon reduction of the -S-S- bond (i.e. PDIs, DTT), fluorescence emission of eosin increases dramatically [25]. The increase in fluorescence signal was monitored at 528 nm with excitation at 485 nm using a Synergy HTX plate reader (Biotek). The total reaction volume was 100 μL. For inhibition of PDIA3 the reaction mixture was incubated with LOC14 (Tocris, 5606) at the indicated concentrations for 30 min on ice prior to the addition of DiE-GSSG. IC50s were calculated using GraphPad Prism (version 7.0, GraphPad); briefly initial rates of fluorescence over time were determined over the first 10 min for indicated inhibitor concentrations, IC50s were then determined using three-parameter non-linear regression.

4.14. Biotin switch assay

To block free sulfhydryls, cells were lysed in buffer containing 20 mM Tris·HCl (pH 8.0), 100 mM NaCl, 0.5% Nonidet P-40, 10% glycerol, 1% protease inhibitor cocktail (Sigma-Aldrich, P8340) (v/v), 1% phosphatase inhibitor cocktails 1 and 2 (Sigma-Aldrich, P5726, P0044) (v/v), and 1 mM N-Ethylmaleimide (NEM) for 1 h at ambient temperature. Excess NEM was then removed via acetone precipitation. Briefly, Acetone was cooled to −20 °C. Four times the sample volume was added to protein samples. Samples were then vortexed and incubated overnight at −20 °C. Precipitated protein was pelleted by centrifugation at 14,000 × *g* for 10 min. The supernatant was aspirated and the resulting pellet was suspended in buffer containing 20 mM Tris·HCl (pH 8.0), 100 mM NaCl, 0.5% Nonidet P-40, 10% glycerol, 1% SDS, and 1% protease inhibitor cocktail (Sigma-Aldrich, P8340) (v/v), 1% phosphatase inhibitor cocktails 1 and 2 (Sigma-Aldrich, P5726, P0044) (v/v). Upon resuspension disulfides were reduced with 20 μM DTT and newly formed sulfhydryl groups were labeled with 1 mM 3-(N-maleimido-propionyl) biocytin (MPB) (Invitrogen, M1602) for 1 h at ambient temperature. Excess DTT and MPB were removed via acetone precipitation. The labeled lysate was precipitated using NeutrAvidin agarose resin (Thermo Scientific, 29200) and subsequently probed using an anti-HA antibody. As a reagent control lysates from cells were incubated with DMSO and subjected to the same procedures.

4.15. Flow cytometry

The following antibodies were used for flow cytometric staining: anti-IAV NP (Abcam, ab20921), Mouse IgG1 isotype control (Abcam, ab91356). Intracellular staining was performed using the BD Cytofix/Cytoperm kit (Becton Dickinson, 554714), according to the manufacturers instructions. All samples were run on a Guava easyCyte HT cytometer (Millipore) and analyzed using Flowjo (version 10.4.2, TreeStar)

4.16. Statistics

Data were analyzed by one-way analysis of variance (ANOVA) and a Tukey's post-hoc test to adjust for multiple comparisons, or student's *t*-test where appropriate. Statistical analysis was performed using Graph Pad Prism (version 7.0, Graph Pad). A p value < 0.05 was considered significant. Data from multiple experiments were averaged and expressed as mean values ± SEM.

4.17. Microarray analysis

GEO2R (www.ncbi.nlm.nih.gov/geo/info/geo2r.html) was used to perform comparisons on differentially expressed genes between influenza-infected samples and normal controls on GSE63786 and GSE48466. GEO2R automatically performs a base 2 log transformation.

4.18. Caspase assay

25 μg of treated MTEC lysate was brought to 25ul with dH2O and 25ul Caspase-Glo 3/7-assay reagent (Promega, G8091) were mixed and incubated in the dark at ambient temperature for 20 min. Total luminescence was monitored using a Synergy HTX plate reader (Biotek). Values were expressed as relative luminescence units.

4.18.1. Small interfering (si)RNA treatment

Mouse type II epithelial cells (C10) were cultured as describe previously [17]. Cells were treated with Accell control small interfering (si) RNA (Dharmacon, D-001920–02-05) or PDIA3 siRNA (Dharmacon, E-045187–00) as per manufactures instructions for 24 h prior to infection with influenza virus or UV-irradiated mock virus.

4.18.2. Immunoprecipitation

HBE cells were lysed in cells were lysed in buffer containing 20 mM Tris·HCl (pH 8.0), 100 mM NaCl, 0.5% Nonidet P-40, 10% glycerol, 1% protease inhibitor cocktail (Sigma-Aldrich, P8340) (v/v), 1% phosphatase inhibitor cocktails 1 and 2 (Sigma-Aldrich, P5726, P0044) (v/v). PDIA3 was precipitated using anti-PDIA3 antibody (Enzo Life Sciences, ADI-SPA-585-F) and Protein G agarose beads (Invitrogen, 15920010). As a control lysates from cells were incubated non-specific rabbit gamma globulin (Jackson ImmunoResearch, 011–000-002) and subjected to the same procedures. Samples were run on reducing gels.

Author summary

Current Influenza virus therapies target viral proteins and are limited in their effectiveness owing to rapid viral mutation. Understanding host cellular and molecular processes utilized by the virus during its replication may aid in the development of new therapeutic interventions to improve patient survival. Influenza proteins such as hemagglutinin (HA) rely on disulfide bonds for stability and activity and as such rely on host redox enzymes of the endoplasmic reticulum (ER) and the secretory pathway to express and assemble fully mature viral proteins. Past work has shown that one of these enzymes, protein disulfide isomerase (PDI) A3 is important for efficient folding of HA and viral replication *in vitro*. However, little is known about how PDIA3 mediates this effect or its role during active viral infection *in vivo*. Here, we demonstrate that PDIA3 is required for productive viral infection *in vivo* using conditional PDIA3 knockout mice. Moreover, we also show that small molecule mediated inhibition of PDIs with the reversible inhibitor LOC14 results in decreased viral replication, inflammation, and oxidative folding of HA. Thus, PDIA3 and other host redox active enzymes may provide targets for future therapies, and LOC14 may provide the basis for novel therapeutic interventions.

CRediT authorship contribution statement

Nicolas Chamberlain: Conceptualization, Data curation, Formal analysis, Investigation, Validation, Visualization, Writing - original draft, Writing - review & editing. **Bethany R. Korwin-Mihavics:** Investigation, Formal analysis. **Emily M. Nakada:** Methodology, Writing - review & editing. **Sierra R. Bruno:** Investigation, Writing - review & editing. **David E. Heppner:** Methodology, Writing - review & editing. **David G. Chapman:** Investigation, Methodology, Writing - review & editing. **Sidra M. Hoffman:** Investigation, Methodology. **Albert van der Vliet:** Methodology, Writing - review & editing. **Benjamin T. Suratt:** Methodology, Writing - review & editing. **Oliver Dienz:** Methodology, Writing - review & editing. **John F. Alcorn:** Conceptualization, Writing - review & editing. **Vikas Anathy:** Conceptualization, Investigation, Methodology, Project administration, Resources, Funding acquisition, Validation, Visualization, Writing - original draft, Writing - review & editing.

Acknowledgments

We thank N. Daphtary and M. Aliyeva for AHR. Imaging work was performed at the Microscopy Imaging Center at the University of Vermont. Confocal microscopy was performed on a Zeiss 510 META laser scanning confocal microscope supported by NIH Award no. 1S10RR019246 from the National Center for Research Resources.

Funding sources

This work is supported by grants from National Institutes of Health grants HL122383 and HL141364, Department of Pathology and Laboratory Medicine and COM IGP at UVM to V. Anathy, HL076122 and P30 GM103532 to the Vermont Lung Center.

V. Anathy and N. Chamberlain have a pending patent application on Protein disulfide isomerase A3 inhibitory compounds and methods of use US APP. NO. 62/661,601.

Appendix A. Supplementary material

Supplementary data associated with this article can be found in the online version at doi:10.1016/j.redox.2019.101129.

References

[1] T. Inoue, B. Tsai, How viruses use the endoplasmic reticulum for entry, replication, and assembly, Cold Spring Harb. Perspect. Biol. 5 (1) (2013) a013250.
[2] N.A. Patil, et al., Cellular disulfide bond formation in bioactive peptides and proteins, Int. J. Mol. Sci. 16 (1) (2015) 1791–1805.
[3] B. Kleizen, I. Braakman, Protein folding and quality control in the endoplasmic reticulum, Curr. Opin. Cell Biol. 16 (4) (2004) 343–349.
[4] W.J. Wedemeyer, E. Welker, M. Narayan, H.A. Scheraga, Disulfide bonds and protein folding, Biochemistry 39 (15) (2000) 4207–4216.
[5] M. Narayan, E. Welker, W.J. Wedemeyer, H.A. Scheraga, Oxidative folding of proteins, Acc. Chem. Res. 33 (11) (2000) 805–812.
[6] S.M. Hoffman, et al., Protein disulfide isomerase-endoplasmic reticulum resident protein 57 regulates allergen-induced airways inflammation, fibrosis, and hyperresponsiveness, J. Allergy Clin. Immunol. 137 (3) (2016) 822–832 (e7).
[7] J.J. Galligan, D.R. Petersen, The human protein disulfide isomerase gene family, Hum. Genom. 6 (6) (2012).
[8] H. Coe, et al., Role of cysteine amino acid residues in calnexin, Mol. Cell Biochem 359 (1–2) (2012) 271–281.
[9] U. Woehlbier, et al., ALS-linked protein disulfide isomerase variants cause motor dysfunction, EMBO J. 35 (8) (2016) 845–865.

[10] F.S. Ramos, et al., PDIA3 and PDIA6 gene expression as an aggressiveness marker in primary ductal breast cancer, Genet Mol. Res. 14 (2) (2015) 6960–6967.
[11] N. Sriwilaijaroen, Y. Suzuki, Molecular basis of the structure and function of H1 hemagglutinin of influenza virus, Proc. Jpn. Acad. Ser. B 88 (6) (2012) 226–249.
[12] T.O. Edinger, M.O. Pohl, S. Stertz, Entry of influenza A virus: host factors and antiviral targets, J. Gen. Virol. 95 (Pt 2) (2014) 263–277.
[13] I. Singh, R.W. Doms, K.R. Wagner, A. Helenius, Intracellular transport of soluble and membrane-bound glycoproteins: folding, assembly and secretion of anchor-free influenza hemagglutinin, EMBO J. 9 (3) (1990) 631–639.
[14] M.S. Segal, Disulfide bond formation during the folding of influenza virus hemagglutinin, J. Cell Biol. 118 (2) (1992) 227–244.
[15] T. Solda, et al., Consequences of ERp57 deletion on oxidative folding of obligate and facultative clients of the calnexin cycle, J. Biol. Chem. 281 (10) (2006) 6219–6226.
[16] M. Pieren, et al., The use of calnexin and calreticulin by cellular and viral glycoproteins, J. Biol. Chem. 280 (31) (2005) 28265–28271.
[17] E.C. Roberson, et al., Influenza induces endoplasmic reticulum stress, caspase-12-dependent apoptosis, and c-Jun N-terminal kinase-mediated transforming growth factor-beta release in lung epithelial cells, Am. J. Respir. Cell Mol. Biol. 46 (5) (2012) 573–581.
[18] A. Kaplan, et al., Small molecule-induced oxidation of protein disulfide isomerase is neuroprotective, Proc. Natl. Acad. Sci. USA 112 (17) (2015) E2245–E2252.
[19] J.E. Shoemaker, et al., An Ultrasensitive mechanism regulates influenza virus-induced inflammation, PLoS Pathog. 11 (6) (2015) e1004856.
[20] R.L. Gerlach, et al., Early host responses of seasonal and pandemic influenza A viruses in primary well-differentiated human lung epithelial cells, PLoS One 8 (11) (2013) e78912.
[21] S. Parakh, J.D. Atkin, Novel roles for protein disulphide isomerase in disease states: a double edged sword? Front Cell Dev. Biol. 3 (2015) 30.
[22] B.G. Hoffstrom, et al., Inhibitors of protein disulfide isomerase suppress apoptosis induced by misfolded proteins, Nat. Chem. Biol. 6 (12) (2010) 900–906.
[23] S. Vatolin, et al., Novel protein disulfide isomerase inhibitor with anticancer activity in multiple myeloma, Cancer Res. 76 (11) (2016) 3340–3350.
[24] S. Xu, et al., Discovery of an orally active small-molecule irreversible inhibitor of protein disulfide isomerase for ovarian cancer treatment, Proc. Natl. Acad. Sci. USA 109 (40) (2012) 16348–16353.
[25] A. Raturi, B. Mutus, Characterization of redox state and reductase activity of protein disulfide isomerase under different redox environments using a sensitive fluorescent assay, Free Radic. Biol. Med 43 (1) (2007) 62–70.
[26] D. Klett, et al., Effect of pharmaceutical potential endocrine disruptor compounds on protein disulfide isomerase reductase activity using di-eosin-oxidized-glutathione, PLoS One 5 (3) (2010) e9507.
[27] S.W. Gerritz, et al., Inhibition of influenza virus replication via small molecules that induce the formation of higher-order nucleoprotein oligomers, Proc. Natl. Acad. Sci. USA 108 (37) (2011) 15366–15371.
[28] M. Laporte, L. Naesens, Airway proteases: an emerging drug target for influenza and other respiratory virus infections, Curr. Opin. Virol. 24 (2017) 16–24.
[29] L. Ellgaard, M. Molinari, A. Helenius, Setting the standards: quality control in the secretory pathway, Science 286 (5446) (1999) 1882–1888 (Dec 3).
[30] R.W. Doms, A. Helenius, Quaternary structure of influenza virus hemagglutinin after acid treatment, J. Virol. 60 (3) (1986) 833–839.
[31] C.S. Copeland, K.P. Zimmer, K.R. Wagner, G.A. Healey, I. Mellman, A. Helenius, Folding, trimerization, and transport are sequential events in the biogenesis of influenza virus hemagglutinin, Cell 53 (2) (1988) 197–209.
[32] N.M. Bouvier, A.C. Lowen, Animal Models for Influenza Virus Pathogenesis and Transmission, Viruses 2 (8) (2010) 1530–1563.
[33] P.M. Vanhoutte, Epithelium-derived relaxing factor(s) and bronchial reactivity, J. Allergy Clin. Immunol. 83 (5) (1989) 855–861.
[34] Y.J. Chang, et al., Innate lymphoid cells mediate influenza-induced airway hyperreactivity independently of adaptive immunity, Nat. Immunol. 12 (7) (2011) 631–638.
[35] P.J. Sterk, Virus-induced airway hyperresponsiveness in man, Eur. Respir. J. 6 (6) (1993) 894–902.
[36] C.G. Irvin, J.H. Bates, Measuring the lung function in the mouse: the challenge of size, Respir. Res. 4 (4) (2003).
[37] T. Watanabe, S. Watanabe, Y. Kawaoka, Cellular networks involved in the influenza virus life cycle, Cell Host Microbe 7 (6) (2010) 427–439.
[38] Y. Kim, K.O. Chang, Protein disulfide isomerases as potential therapeutic targets for influenza A and B viruses, Virus Res 247 (2018) 26–33.
[39] M.D. Tate, et al., Playing hide and seek: how glycosylation of the influenza virus hemagglutinin can modulate the immune response to infection, Viruses 6 (3) (2014) 1294–1316.
[40] S. Tong, X. Zhu, Y. Li, M. Shi, J. Zhang, M. Bourgeois, H. Yang, X. Chen, S. Recuenco, J. Gomez, L.M. Chen, A. Johnson, Y. Tao, C. Dreyfus, W. Yu, R. McBride, P.J. Carney, A.T. Gilbert, J. Chang, Z. Guo, C.T. Davis, J.C. Paulson, J. Stevens, C.E. Rupprecht, E.C. Holmes, I.A. Wilson, R.O. Donis, New world bats harbor diverse influenza A viruses, PLoS Pathog. 9 (10) (2013).
[41] C.S. Copeland, Assembly of influenza hemagglutinin trimers and its role in intracellular transport, J. Cell Biol. 103 (4) (1986) 1179–1191.
[42] H.D. Klenk, W. Garten, Host cell proteases controlling virus pathogenicity, Trends Microbiol. 2 (2) (1994) 39–43.
[43] S. DA, Role of hemagglutinin cleavage for the pathogenicity of influenza virus, Virology 258 (1) (1999) 1–20.
[44] M.J. Gething, K. McCammon, J. Sambrook, Expression of wild-type and mutant forms of influenza hemagglutinin: the role of folding in intracellular transport, Cell 46 (6) (1986) 939–950.
[45] M.J. Gething, Role and regulation of the ER chaperone BiP, Semin Cell Dev. Biol. 10 (5) (1999) 465–472.
[46] Y. Ma, L.M. Hendershot, ER chaperone functions during normal and stress conditions, J. Chem. Neuroanat. 28 (1–2) (2004) 51–65.
[47] L. Ellgaard, A. Helenius, Quality control in the endoplasmic reticulum, Nat. Rev. Mol. Cell Biol. 4 (3) (2003) 181–191.
[48] F.F. Dias, et al., Human eosinophil leukocytes express protein disulfide isomerase in secretory granules and vesicles: ultrastructural studies, J. Histochem Cytochem 62 (6) (2014) 450–459.
[49] Z. Xiao, et al., Molecular mechanisms of glutaredoxin enzymes: versatile hubs for thiol-disulfide exchange between protein thiols and glutathione, J. Mol. Biol. 431 (2) (2019) 158–177.
[50] E.S. Arner, Focus on mammalian thioredoxin reductases–important selenoproteins with versatile functions, Biochim. Biophys. Acta 1790 (6) (2009) 495–526.
[51] R. Sgarbanti, et al., Redox regulation of the influenza hemagglutinin maturation process: a new cell-mediated strategy for anti-influenza therapy, Antioxid. Redox Signal 15 (3) (2011) 593–606.
[52] Z. Hantos, B. Daroczy, B. Suki, S. Nagy, J.J. Fredberg, Input impedance and peripheral inhomogeneity of dog lungs, J. Appl. Physiol. 72 (1) (1992) 168–178.
[53] S. Tomioka, J.H. Bates, C.G. Irvin, Airway and tissue mechanics in a murine model of asthma: alveolar capsule vs. forced oscillations, J. Appl. Physiol. 93 (1) (2002) 263–270.
[54] L.K. Lundblad, et al., Airway hyperresponsiveness in allergically inflamed mice: the role of airway closure, Am. J. Respir. Crit. Care Med 175 (8) (2007) 768–774.
[55] D.A. Ellerman, D.G. Myles, P. Primakoff, A role for sperm surface protein disulfide isomerase activity in gamete fusion: evidence for the participation of ERp57, Dev. Cell 10 (6) (2006) 831–837.
[56] J. Chen, et al., Protein-disulfide isomerase-associated 3 (Pdia3) mediates the membrane response to 1,25-dihydroxyvitamin D3 in osteoblasts, J. Biol. Chem. 285 (47) (2010) 37041–37050.
[57] C. Turano, et al., Proteins of the PDI family: unpredicted non-ER locations and functions, J. Cell Physiol. 193 (2) (2002) 154–163.
[58] A.K. Perl, L. Zhang, J.A. Whitsett, Conditional expression of genes in the respiratory epithelium in transgenic mice Cautionary Notes and Toward Building a better mouse trap, Am. J. Respir. Cell Mol. Biol. 40 (1) (2009) 1–3.
[59] A.-K.T. Perl, et al., Conditional Recombination Reveals Distinct Subsets of Epithelial Cells in Trachea, Bronchi, and Alveoli, Am. J. Respir. Cell Mol. Biol. 33 (5) (2005) 455–462.
[60] N. Garbi, et al., Impaired assembly of the major histocompatibility complex class I peptide-loading complex in mice deficient in the oxidoreductase ERp57, Nat. Immunol. 7 (1) (2006) 93–102.
[61] S.M. Hoffman, J.E. Tully, J.D. Nolin, K.G. Lahue, D.H. Goldman, N. Daphtary, M. Aliyeva, C.G. Irvin, A.E. Dixon, M.E. Poynter, V. Anathy, Endoplasmic reticulum stress mediates house dust mite-induced airway epithelial apoptosis and fibrosis, Respir. Res. 14 (141) (2013).